Journal of Geography, Environment and Earth Science International
4(1): 1-13, 2016; Article no.JGEESI.20488
ISSN: 2454-7352

SCIENCEDOMAIN *international*
www.sciencedomain.org

Global Distribution of Zones of Enhanced Risk for the Ionospheric Weather

T. L. Gulyaeva[1*], F. Arikan[2], I. Stanislawska[3] and L. V. Poustovalova[1]

[1]Institute of Terrestrial Magnetism, Ionosphere and Radio Wave Propagation, IZMIRAN, Kaluzskoe Sh. 4, Troitsk, Moscow, 142190, Russia.
[2]Department of EEE, Hacettepe University, Beytepe, Ankara 06800, Turkey.
[3]Space Research Center, PAS, Barticka 18-A, Warsaw, Poland.

Authors' contributions

This work was carried out in collaboration between all authors. Author TLG designed the study, performed the statistical analysis and wrote the first draft of the manuscript. Author FA managed the literature searches and improved the draft of manuscript. Author IS managed the experimental process and author LVP provided maps transformation. All authors read and approved the final manuscript.

Article Information

DOI:10.9734/JGEESI/2016/20488
Editor(s):
(1) Wen-Cheng Liu, Department of Civil and Disaster Prevention Engineering, National United University, Taiwan and Taiwan Typhoon and Flood Research Institute, Taipei, Taiwan.
Reviewers:
(1) Washington L. F. Correia Filho, Universidade Federal do Rio Grande do Norte, Brazil.
(2) Abubakar Yakubu, Universiti Putra, Malaysia.
Complete Peer review History: http://sciencedomain.org/review-history/11617

Original Research Article

Received 30th July 2015
Accepted 14th September 2015
Published 29th September 2015

ABSTRACT

Regions of the permanent ionosphere instability are identified with 24h daily global W-index maps produced from Global Ionospheric Maps of Total Electron Content, GIM-TEC, provided by Jet Propulsion Laboratory. Planetary Wp index derived from hourly W-index maps from January, 1999, to present, is used to compile Catalogue of more than 270 ionospheric storms which comprise 8% of total database, and the rest represents quiet conditions. The positive storm percentage occurrence (enhanced electron density, pW^+) and negative storm occurrence (depleted electron density, pW^-) are analyzed in space and time showing dependence on solar activity (SA) and seasons for the global ionosphere and its adopted 240 sub-domains (of latitude bins equal to 10º in the polar regions and 20° elsewhere and 15° hourly longitude bins). A global occurrence of pW^+ and pW^- during Wp storms follows the 11-year solar cycle with pW^- greater than pW^+ by about 2 times at high SA and moderate SA while the opposite is observed at solar minimum when pW^+ is

**Corresponding author: Email: gulyaeva@izmiran.ru;*

greater than pW^- by about 1.2 times. The regions of enhanced positive storm activity (pW^+≈10%) are found to occur in the South America, North seashores of Europe and Russia, and between longitudes 30°W to 30°E in Antarctica. Zones of negative storms (pW^-≈22%) are dominated in Antarctica. The pW^+ and pW^- depict winter maximum of pW^+ and summer maximum of pW^- under Wp storm conditions decreasing from high latitudes to minimum at equator throughout all seasons in the both hemispheres. While pW^+ and pW^- reach 20-25% under the ionosphere storm conditions, the spatial occurrence of pW^+ and pW^- comprise 6% under quiet conditions at high latitudes which testify on the persistent plasma instability in the ionosphere through more than the total cycle of solar activity.

Keywords: Ionospheric weather; global ionospheric map; total electron content; w-index; ionospheric storm.

1. INTRODUCTION

An increased knowledge of effects imposed by the ionosphere on operational radio systems could be gained by the new service providing online estimate of the degree of ionosphere perturbation expressed by the ionospheric W index at each grid point of the Global Ionospheric Map of Total Electron Content, GIM-TEC. Total Electron Content (TEC) is one of the main parameters that defines the structure of the ionosphere. TEC represents the total number of electrons along a tube of 1 m^2 cross section between receiver and satellite upto the satellite orbit at 20,000 km over the Earth. Products of GIM-TEC become possible with the emergence of the Global Navigation Satellite System (GNSS) which has opened new opportunities for studying the spatial distribution and temporal evolution of the ionosphere. The GNSS-based global and regional ionosphere TEC maps serve as the database for numerous investigations on the morphology and dynamics of the ionosphere [1-9]. Based on GIM-TEC, the differential TEC maps present an option for a measure of the spatial and temporal developments of a space weather induced perturbation pattern [10].

While TEC measurements at GPS-receivers sites are more accurate compared with spatially- and temporally-smoothed GIM-TEC products, the GIM data are readily available for investigating global characteristics of the ionosphere. Besides, it is well recognized that uneven GNSS receiver network located mainly on the land and islands over the globe imposes interpolation/ computational problems in maps production for the large caveat areas over the oceans [4,11]. However, while the interpolated TEC values over the oceans may suffer in accuracy as compared with data available in inhabited areas, the relative TEC variability is congruent with variability of the ionospheric TEC measured onboard the Topex/Jason satellites over the ocean [12].

Recently developed system of the ionospheric W index as a measure of the ionosphere variability with magnitude varying along the integer scale from W = -4 (strong negative ionospheric storm) through W = 0 (quiet conditions) to W = 4 (strong positive ionospheric storm) allows to distinguish the state of ionosphere and plasmasphere from quiet conditions to the intense storms (Table 1), ranging the plasma density from enhancements (positive phase) to depletions (negative phase) with respect to the quiet reference or normal state [11,13-15]. So defined W index differs from the relative deviation of the ionospheric F2 layer critical frequency, the peak electron density or TEC from the quiet reference which don't provide a uniform measure of the ionosphere disturbances because positive relative deviations are deeper than negative ones [16]. GIM-TEC maps, provided by Jet Propulsion Laboratory in the IONEX format (-87.5°:2.5°:87.5° in latitude, -180°:5°:180° in longitude) are used as the database for deriving the W-index maps from 1999 to present.

Procedure for derivation of planetary Wp index from W-index map [13] is provided in Section 2, accompanied by criteria for the principal properties of Wp index characterizing the global ionosphere storm. Wp index is generated from more than 139,000 sample W-index maps between 1999 and 2015. According to proposed criteria for Wp index storm specification, we produce for the first time Catalogue of more than 270 ionospheric storms for more than sixteen years of observation which includes the storms comprising 8% of total database, and the rest representing the quiet conditions.

This study is focused on global evaluation of occurrence of the ionosphere storm in space and time extending investigations carried out so far with different approaches [3,5-7,9,17,18]. The ionosphere disturbances under quiet geomagnetic conditions are discussed in literature in various studies including but not limited to those presented by [14,19,20]. Since the Catalogue of the ionosphere storms is compiled recently, the ionospheric storm signatures under non-storm conditions are specified in the present study for the first time in the literature.

2. DATA ANALYSIS

The Degree of perturbation of Total Electron Content, DTEC, at each grid point (φ_i, λ_i) of the ionosphere map (2.5°×5.0° in latitude, φ, and longitude, λ, respectively) is computed as logarithm of TEC relative to quiet reference. We choose a quiet 7-day prior median value for each UT hour (0, 1,…,23 h UT) as a quiet TEC which is assigned to the hour UT at the day of observation. Though in many cases the quiet period is centered on the current day [3], usage of deviation of an instant value from the quiet background median for the preceding period is important for the forecasting purposes when only prior data are available for the current day [9, 11]. It is assumed, that value of W at grid point (φ_i, λ_i) is valid also in the surrounding rectangular section of the IONEX map, i.e. it is valid from φ_i - 1.25º to φ_i + 1.25º in latitude, and from λ_i - 2.5º to λ_i + 2.5º in longitude. The W-index map is generated by segmentation of DTEC with the relevant thresholds given in Table 1 so that the local W index equal to 0, 1 or −1 stands for the quiet state, 2 or −2 for the moderate disturbance, 3 or −3 for the moderate ionospheric storm, and 4 or −4 for intense ionospheric storm at each grid point of the map similar to the F2 layer peak electron density, NmF2, related with the critical frequency, foF2 [11,13].

The planetary ionospheric storm Wp index is obtained from W-index map derived from GIM-TEC as a latitudinal average of the span between maximum positive and minimum negative W-index weighted by the latitude/longitude extent of the extreme values on the map [13]. Since the occurrence of positive and negative indices depends on season, location, external forces, intensity and local starting time of a perturbation, we take the advantage of a round-the-world longitudinal presentation (24 h LT) of the index at the latitude which allows us to investigate zones of enhanced risk of the ionospheric storm occurring at any local time.

The difference (span) between the maximum of positive index, *Wmaxj*, and the minimum of negative index, *Wminj*, at the *j*-th latitude, serves as a latitudinal measure of the storm if there are values corresponding to the storm at the particular latitude (Eq. 1a) or otherwise (Eq. 1b):

$$\delta Wj = W\max j - W\min j \text{ for } Wmaxj \geq 3 \text{ and/or } Wminj \leq -3 \tag{1a}$$

$$\delta Wj = \max(W\max j, |W\min j|) \text{ for } Wmaxj \leq 2 \text{ and } Wminj \geq -2 \tag{1b}$$

The planetary Wp index depicts contributions of perturbation at a global scale as

$$Wp = \left(1 + k \times n^{-1} \times m^{-1}\right) \times n^{-1} \sum_{j=1}^{n} \delta Wj \tag{2}$$

Table 1. Categories of the ionospheric weather W-index corresponding to the logarithmic deviation of total electron content, TEC, from the median: DTEC = log(TEC/TECmed)

W-index	DTEC	Ionospheric state
4	DTEC > 0.301	Intense positive W^+ storm
3	0.155 < DTEC ≤ 0.301	Moderate W^+ storm or substorm
2	0.046 < DTEC ≤ 0.155	Moderate W^+ disturbance
1	0.0 < DTEC ≤ 0.046	Quiet W^+ state
0	DTEC = 0.0	Reference Quiet state
-1	-0.046 ≤ DTEC < 0.0	Quiet W^- state
-2	-0.155 ≤ DTEC < -0.046	Moderate W^- disturbance
-3	-0.301 ≤ DTEC < -0.155	Moderate W^- storm or substorm
-4	DTEC < -0.301	Intense negative W^- storm

where *Wp* is the latitude averaged span between extreme values of *Wj* at each latitude *j*. Parameter *n* represents number of grid latitudes (*n* = 71 for IONEX map), and *m* – number of grid longitudes (*m* = 72) on a map. The weight $(1+k \times n^{-1} \times m^{-1})$ in Eq. (2) explains the latitude-longitude extent of the areas of the greatest positive index *Wmax = max(Wmaxj)*, and the least negative value *Wmin = min(Wminj)*. Parameter *k* represents total number of the extreme positive W indices (W = 3 and 4) and negative W indices (W= -3 and -4) on a map.

As distinct from the positive and negative local W-index specified in all cells of a map, the differential planetary Wp index is always positive varying from 1.0 (when none storm W index is present on a map, *k* = 0) to 10.0 i.u. (index units) specifying the ionosphere from the quiet times when Wp < 3.0 i.u. to the planetary ionosphere storm times when Wp ≥ 3.0 i.u. The upper limit of maximum Wp =16.0 i.u. could be calculated formally substituting maximum $k = n \times m$, and maximum $\delta Wj = 8$ (span between $W^+ = 4$ and $W^- = -4$ at each latitude of a map); however, in reality it never occurs that the peak positive W index is equal to '4' at all latitudes of the map simultaneously with the negative W index equal to '-4' at all latitudes of the same map, so the actual limit of Wpmax ≤ 10.0 i.u. is determined empirically from the total W-index database.

Planetary Wp index is calculated from hourly W-index maps constituting total database of more than 140,000 hourly values of Wp for the period from January, 1999, to June, 2015. The original JPL GIM-TEC maps available with 2-h step before 2008 (and 1-h afterwards) have been linearly interpolated to 1-h resolution before W-index map processing. Percentage distribution of Wp index within ten ranges of Wp index unit relative to total Wp data set for 1999-2014 is presented in Table 2.

While from Table 2 one can see that the total number of cases of Wp ≥ 3 i.u. is about 30% of the whole database, the ionosphere storm is specified by the criteria for a period when the following significant thresholds / conditions are satisfied:

i) successive UT-hourly Wp values are greater or equal to 3.0 i.u.;
ii) maximum of Wp is equal to or greater than *Wpmax* = 5.0 i.u.;
iii) storm time duration satisfying thresholds (1) and (2) is 5 hours or longer.

The storm duration of at least 5 h eliminates incidental hour-to-hour global TEC variations and includes at least two original GIM-TEC maps with 2-h temporal resolution before 2008.

Based on Wp index filtered with the above storm criteria, Catalogue of the ionosphere storms is compiled for the first time in the ionosphere research consisting of more than 270 events from January 1999 to June 2015 which is permanently updated if new products of Wp index capture a storm. With 24 hourly W-index maps a day over more than 16 years, there are more than 140,000 sample maps, 8% of which comprise Wp storm times, and the rest 92% represents the quiet conditions. These proportions are very similar to those values for storm and quiet TEC maps associated with the intense ring current Dst storms [7]. In this study, W-index maps are analyzed separately for the Wp-storm conditions and the rest W-index maps termed as 'quiet' or 'non-storm' conditions.

3. POSITIVE AND NEGATIVE IONOSPHERE STORM ANALYSIS

While magnitude of the planetary differential Wp index is always positive, the disturbances in the ionosphere involve enhancement and depletion in electron density and electron content, termed as positive and negative ionospheric storms, respectively. To analyze the both phases of the ionosphere storm, the occurrence of the positive storm indices $W^+ = 3$ and 4 (pW^+) over a specified area can provide spatial characteristic of the positive ionosphere storm and the occurrence of the negative storm indices $W^- = -3$ and -4 (pW^-) can provide characteristic of the spatial occurrence of the negative ionosphere storm [21]. The percentage occurrence of the positive pW^+ and negative pW^- storm W-indices is deduced from the ionospheric activity W-index maps produced from the global ionosphere maps of total electron content of Jet Propulsion Laboratory, GIM-TEC, for 1999-2014.

In this study, the input data are arranged in 10 spatial ranges of latitude and 24 ranges of longitude according to an assumption that each W-index is also valid in the surrounding cell-size space around the grid. The latitudes for the sub-domains are specified as follows: starting from -88.75° to -78.75° (with step size of $\Delta\varphi$ = 10º), eight latitude ranges located from -78.75° to 78.75° in steps of $\Delta\varphi$ = 20°, and finally from 78.75° to 88.75°N (with step size of $\Delta\varphi$ = 10º).

The longitudes for sub-domains are: from -7.5º to 7.5º, from 7.5° to 352.5°E in step $\Delta\lambda$ = 15° that represent 1h bins of local times. The total global map is divided into 240 spherical rectangular sub-domains for evaluation and analysis of an occurrence of positive and negative storm W indices therein. The percentage occurrence of positive storm index W = 3 and 4 (pW^+) and the negative storm index W = -3 and -4 (pW^-) in any sub-domain or the global ionosphere is evaluated with expressions:

$$pW^+ = n(+3,+4)/n \times 100 \quad (3a)$$

$$pW^- = n(-3,-4)/n \times 100 \quad (3b)$$

where $n(+3,+4)$ is number of positive storm index W = 3 and 4, $n(-3,-4)$ is number of negative storm index W = -3 and -4, and n is number of grid points of a specified sub-domain or the total number of grids (n = 5112) in IONEX formatted W-index map.

The annual mean probability of negative and positive ionospheric storms are mapped in Figs. 1a and b, respectively, estimated in 240 sub-domains of the map during Wp storms observed in 2001. Dominant probability of positive and negative ionosphere storms is evident in the auroral zones with probability of the negative storm 1.5 times greater than that of the positive storm. The both maps in Figs. 1a and b show greater probability of occurrence of the ionosphere storms in Antarctic than in Arctic which can serve as a new evidence to possible mechanisms of the ionospheric storms having hemispheric differences (as opposed to simply seasonal differences) in how solar wind energy is transmitted through the magnetosphere into the thermosphere-ionosphere system [22].

Two-dimensional W-index maps are proven to be very informative in identifying the strength and distribution of disturbance. These maps can be utilized in spatio-temporal characterization of storm structures. An example of GIM-TEC and W-index maps for the peak of the Wp storm on 19th February, 2014, at 10:00 h UT is given in Fig. 2a and 2b. The areas of an enhanced electron content (W = 3 and 4, red) and areas of depleted TEC (W = -3 and -4, blue) can be easily observed in Fig. 2b. The instant percentage occurrence of negative storm W index, pW^-, for 240 sub-domains of latitude and longitude are plotted in Fig. 2c, and the percentage occurrence of the positive storm, pW^+, in Fig. 2d. It is observed from Fig. 2d that the positive storm covers 60% to 100% of the Northern hemisphere winter dusk area around East-Asia between 60º and 140°E, a large nighttime latitudinal zone from the North Pole to 40°S over the Pacific Ocean, and North and South America. At the same time, 100% negative storm (Fig. 2c) is observed in summer at Antarctica when sunlight illuminates the ionosphere 24 h a day. Fig. 2 demonstrates the effectiveness of evaluation of an intensity and space location of the positive and negative ionospheric storm characteristics pW^+ and pW^- from W-index maps.

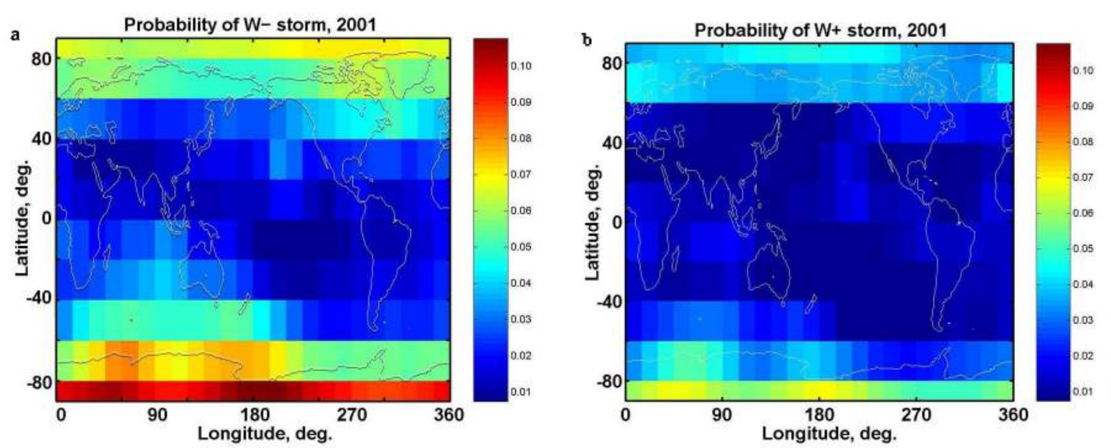

Fig. 1. The annual mean probability of (a) negative and (b) positive ionospheric storms estimated in 240 sub-domains on the W-index maps during ionospheric storms observed in 2001

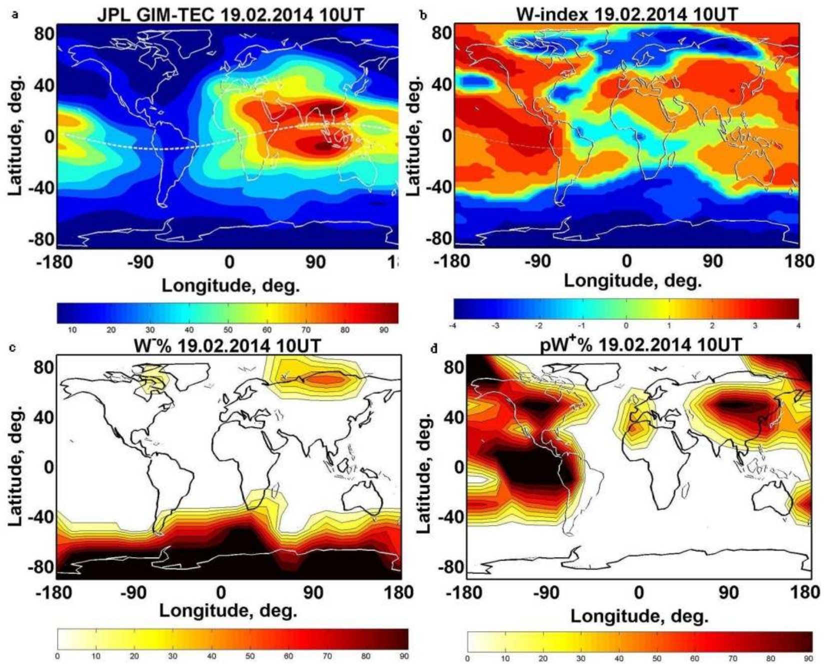

Fig. 2. Characteristics of the peak of the ionosphere storm on 19.02.2014 10:00 UT: a) Global TEC map (TEC=$10^{16}\cdot m^{-2}$); b) W-index map; c) the percentage occurrence of pW^-; d) the percentage occurrence of pW^+

Table 2. Percentage distribution of Wp index in different ranges of index unit (i.u.) relative to the total number of more than 140,000 hourly Wp-index values from January, 1999, to June, 2015

Range of i.u.	1:2	2:3	3:4	4:5	5:6	6:7	7:8	8:9	9:10	≥10
nWp, %	2.826	68.240	22.338	4.476	1.353	.513	.177	.063	.013	.001

A time series of the global percentage occurrence of pW^+, pW^-, and Wp index are plotted in Fig. 3 for the storm from 18 to 21 February, 2014, the same event which instant peak is mapped in Fig. 2. While occurrence of ionosphere storm at specified sub-domains in Figs. 2c and d can reach 100%, Fig. 3 exhibits maximum occurrence of pW^+ up to 25% of the total globe surface and an extreme depletion of pW^- covering 27% of the map at the peak of Wp storm. Geomagnetic Dst index exhibits the double-peak geomagnetic storm coherent with the ionosphere storm signatures.

Monthly mean and annual mean percentage occurrences of the positive and negative W-index storms are given in Fig. 4 congruent with solar activity indicated by the annual sunspot number (SSN) curve. The pW^- exceeds pW^+ by about 2 times for high and moderate solar activity while pW^+ is 1.2 times larger than pW^- for the deep solar minimum of 2007-2009. Re-distribution of positive-to-negative storm occurrence at transition from the solar maximum to minimum is due to the lower background total electron content at solar minimum when the logarithmic deviation of instant TEC from the reference TEC-median can yield greater positive W-index occurrence than that of the negative W-index. In general, the intensity of W-index storms increases with increasing solar activity similar to the occurrence of geomagnetic storms [23].

Spatial intensity of positive and negative storms (Eq. 3a, b) under ionospheric storm and non-storm conditions are mapped in Figs. 5a, b, c, d. During the Wp storms, zones of dominant negative storms (pW^-≈22%) are observed over Antarctica which may be due to particle precipitation (Fig. 5a). The zones of enhanced positive storm activity (pW^+≈10%) are apparent in the South America, North seashores of Europe and Russia, and between longitudes 30°W and 30°E in Antarctica (Fig. 5b). Earlier the dependence of variability of the ionosphere peak electron density on corrected magnetic latitude is investigated by Fotiadis and Kouris [24] who produced an empirical model of four zones of uniformly distributed variability in the 24 h period. Also it has been pointed out that the amplitude of positive ionospheric storms near the peak of equatorial anomaly varies substantially with longitude [8] affected by the vertical drifts primarily driven by meridional neutral winds blowing toward the equator from the hot auroral regions where Joule and particle heating is produced by continuous geomagnetic activity. The areas of enhanced positive storm W-index (Fig. 5b) may be affected by non-migrating tides in the tilted ionosphere at the transition across seashores from sea to land with dominant plasma density and peak height over the sea [12,25].

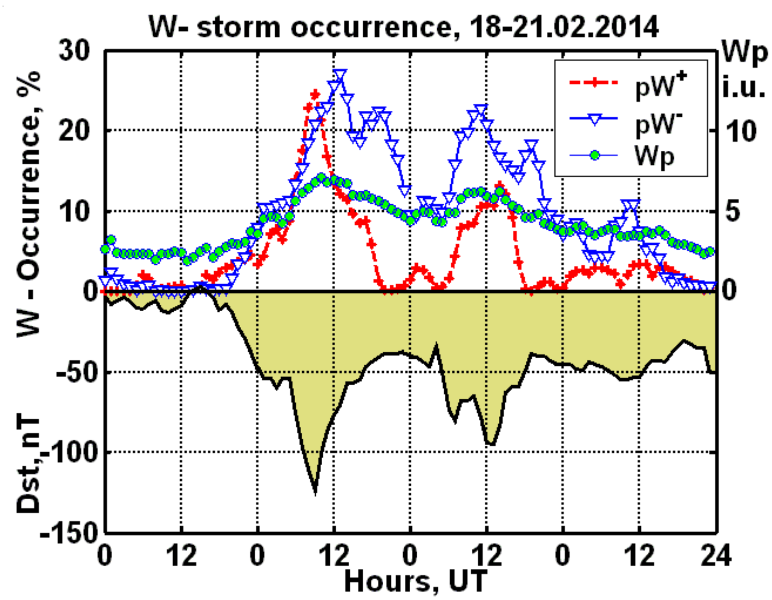

Fig. 3. Global percentage occurrence of pW$^+$, pW$^-$, and Wp index for the W-index storm between 18 to 21 February, 2014, and geomagnetic Dst index

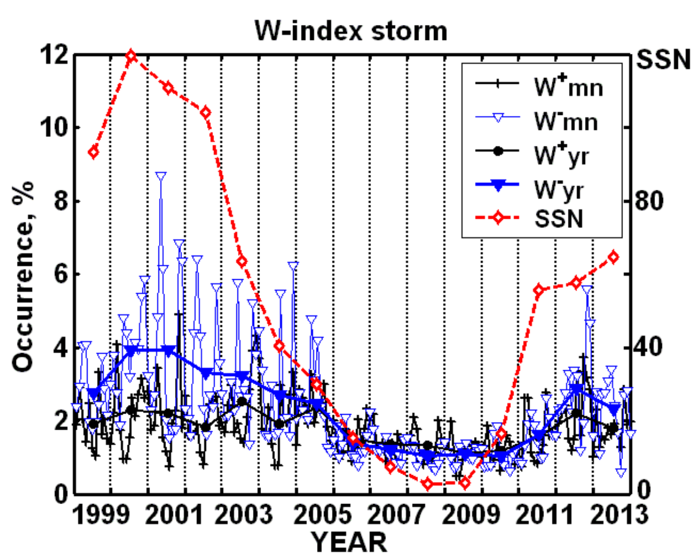

Fig. 4. Monthly mean and annual mean percentage occurrences of the positive and negative W-index storms and the sunspot number, SSN, from 1999 to 2013

We assume that the plasma exchange along the magnetic field lines facilitated during the ionospheric storm may depend on geometry of the sea / land ends of the magnetic line-of-force tubes. Fig. 6a demonstrates the geometry of the magnetic conjugate points having the both ends of line-of-force located either at the continents (green points) or the ocean (blue points) while those areas with the opposite sea–to–land magnetic conjugate pairs not sampled. The zones of an enhanced positive storm activity (Fig. 5b) in the North Europe and Russia, South America and part of Antarctica present areas which might be affected by the dominant plasma fluxes from the ionosphere over the ocean to the magnetic conjugate continental ionosphere. The zones of enhanced ionospheric storm activity may be linked to a possible presence of the inhomogeneity of geomagnetic morphology [26], e.g. the Brasilian magnetic anomaly might be a source for the enhanced positive W-index storm signatures in the South America.

Though less intense in magnitude than above results but $pW^{-}\approx 5\%$ (Fig. 5c) and $pW^{+}\approx 4\%$ (Fig. 5d) occur throughout the total Antarctica under non-storm (quiet) conditions. Note that results of Fig. 5a and 5b are global averages from 8% (about 11,000) of W-index maps for 16 years, and results of Fig. 5c and 5d are global averages from 92% (about 128,000) of W-index maps. The persistent presence of the storm W-indices under non-storm (‘quiet’) conditions over Antarctica deserves special attention. Their intensity could vary on hour-to-hour and day-to-day scales exceeding the total averages for 16 years of observation.

Temporal profiles of the intense positive and negative storm occurrence are plotted in Fig. 7 separately in selected zones of magnetic latitudes (Fig. 6b) for the North and South magnetic hemispheres. These curves are obtained by superposed epoch analysis from W-index storm subset for 1999-2014 with zero time t_0 put at the Wp storm onset. Twice as much peak of the negative ionospheric storm occurrence is obtained as compared with the positive counterpart, in particular, in the polar and sub-auroral magnetic latitudes in the both magnetic hemispheres. The enhanced ionosphere storms and non-storms activity in the Polar Regions is related with the magnetosphere structure which has an open field lines at geomagnetic latitudes above the auroral oval. The closed field lines at middle and low latitudes protect the atmosphere and ionosphere from the interplanetary particles penetration.

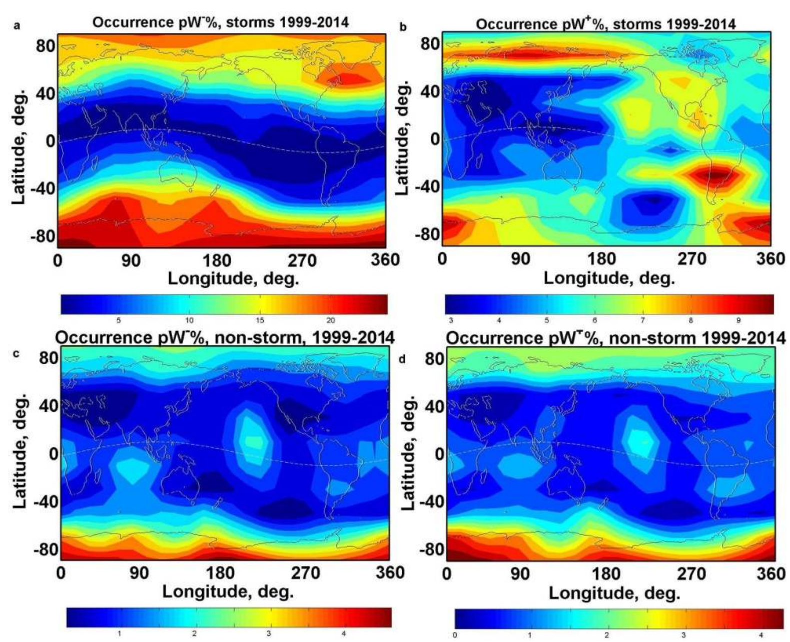

Fig. 5. Spatial distribution a) pW^{-} for storm conditions, b) pW^{+} for storm conditions, c) pW^{-} for non-storm conditions, d) pW^{+} for non-storm conditions

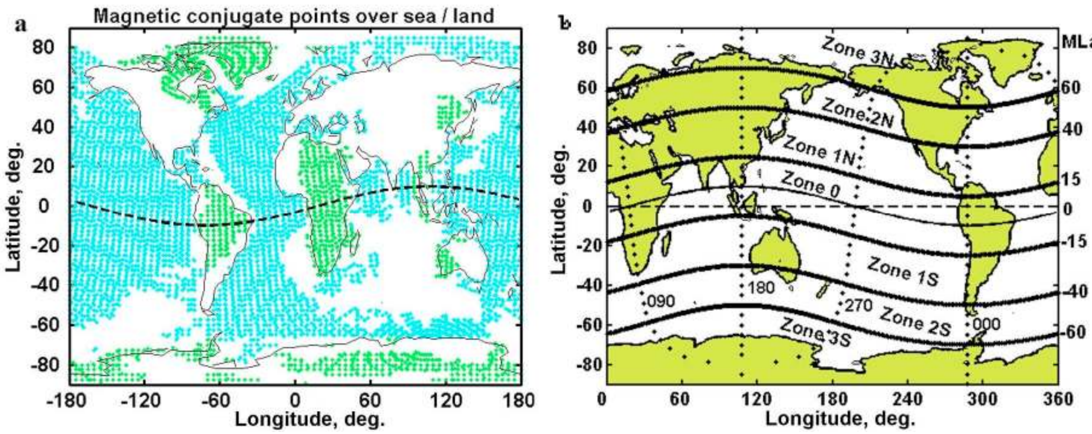

Fig. 6. (a) Global distribution of magnetic conjugates counterparts with the both ends of magnetic field line located over continents (green ponts) or oceans (blue points), and the opposite ground-to-sea line-of-force ends area not sampled. (b) Eight magnetic latitude zones with different characteristic of W-index storm occurrence

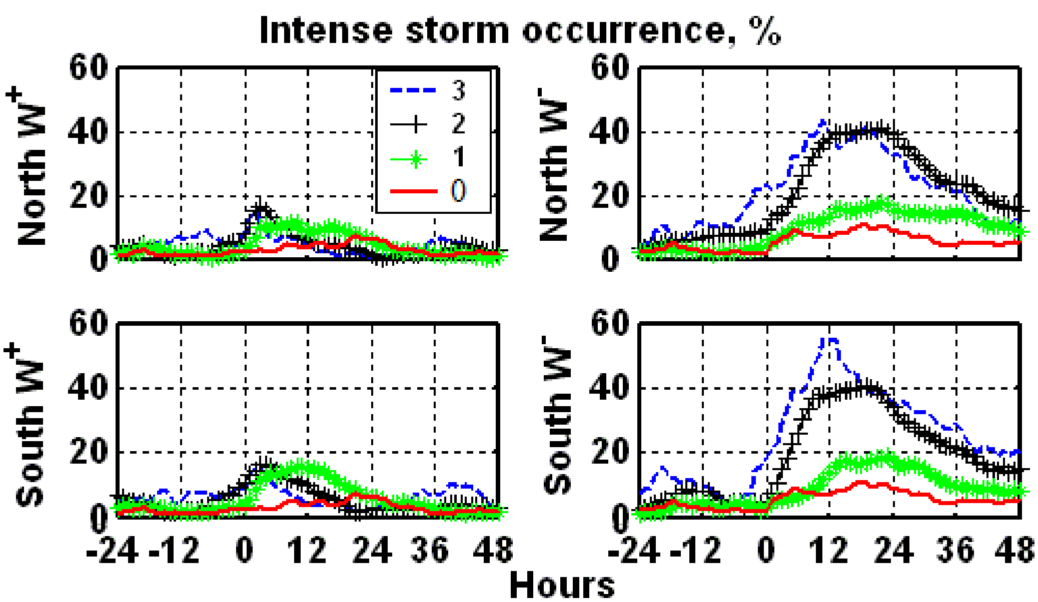

Fig. 7. Percentage occurrence of the positive and negative W-index storms at selected magnetic latitude zones in the North and South magnetic hemispheres for 1999-2014

Seasonal variation of positive pW^+ and negative pW^- occurrence is combined for the relevant seasons in two hemispheres and plotted in Figs. 8a and 8b for the Wp storms and Figs. 8c and 8d for non-storm conditions, respectively. Equinox (eqn) results are collected and averaged for 16 years during March, April, September and October. Winter (wnt) results are compiled for November, December, January and February (North hemisphere sub-domains) and May, June, July and August (South hemisphere sub-domains). Summer (smr) results are compiled for November, December, January and February (South hemisphere sub-domains) and May, June, July and August (North hemisphere sub-domains). All seasonal storm intensities decrease to minimum from high latitudes to equator for all seasons in both hemispheres.

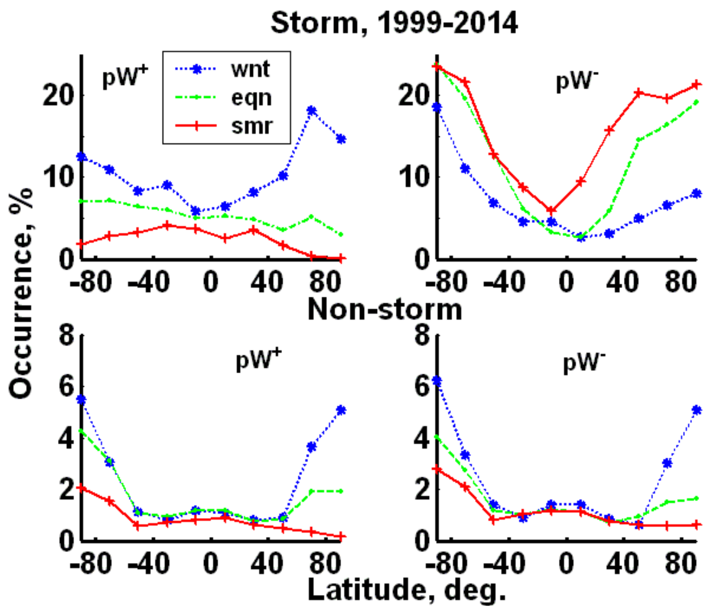

Fig. 8. Seasonal-latitudinal variation of occurrence of the positive and negative ionospheric storms: a) pW$^+$ for storm conditions, b) pW$^-$ for storm conditions, c) pW$^+$ for non-storm conditions, d) pW$^-$ for non-storm conditions

The denser electron density and consequently higher total electron content at sub-equatorial latitudes may affect the relatively less logarithmic deviation from the quiet background values which result in a reduced ionosphere variability at the lower latitudinal zone. As distinct from geomagnetic activity which peaks at the equinoxes [27] the pW$^+$ and pW$^-$ do not depict equinoctial maximum and all equinoctial curves lay in between the winter and summer curves. Here the winter maximum of pW$^+$ (Fig. 8a) and summer maximum of pW$^-$ (Fig. 8b) are obtained under Wp storm conditions. An excess of winter results over summer results is observed for non-storm conditions both with positive and negative storm indices (Figs. 8c and d) but the difference between three seasons become negligible at low and equatorial latitudes from 45°S to 45°N. The largest percentage occurrence is obtained with negative storm signatures at Wp storms in Fig. 8b.

According to [19,28] the high- and mid-latitude positive and negative non-storm Q-disturbances in the F2-region are mainly due to the atomic oxygen concentration variations presumably resulted from the vertical gas motion in the thermosphere and lower atmosphere, including the heights of the ionospheric E-region. The non-storm disturbances of the total electron content shown in Figs. 5c and d and Figs. 8c and d may be also related with the lower layers in the atmosphere. The complementary opportunity on the impact of the ionosphere storms and non-storm disturbances on the weather and climate in the lower atmosphere could be considered for the future work.

4. CONCLUSION

1. In this study, the extent and intensity of the positive and negative ionosphere storms averaged over the globe in 240 sub-domains of a map (of latitude bins equal to 10º in the polar regions and 20° elsewhere and 15° hourly longitude bins) are evaluated. The 24 h global W-index maps are produced from Global Ionospheric Maps of Total Electron Content, GIM-TEC provided by Jet Propulsion Laboratory for 1999-2015. Planetary Wp index generated from W-index map serves as a source of Catalogue of more than 270 ionospheric storms derived from more than 140,000 sample hourly UT maps, 8% of which comprise Wp storm times, and the rest represent the non-storm (quiet) conditions.
2. The percentage occurrence pW$^+$ of positive ionosphere storm (W = 3 and 4) and pW$^-$ for the negative storm (W = -3 and -4) are analyzed under Wp storm and non-storm conditions. While intensity of ionosphere storm at specified sub-domains

of an instant map can reach 100%, average enhancement near 25% of pW^+ for the global ionosphere and depletion 27% of pW^- are obtained under Wp storm conditions. A global occurrence of pW^+ and pW^- during Wp storms follows the 11-years solar cycle with pW^- approximately two times larger than pW^+ at high and moderate solar activity but pW^+ approximately 1.2 times larger than pW^- at extended solar minimum between 2007 and 2009.

3. Zones of enhanced positive storm activity ($pW^+\approx10\%$) are observed in the South America, North seashores of Europe and Russia, and between longitudes 30°W and 30°E in Antarctica, while zones of dominant negative storms ($pW^-\approx22\%$) are observed at Antarctica. Zones of enhanced positive storm activity over the continents may be overflowed by plasma fluxes along the magnetic field lines originated at the conjugate counterparts of greater plasma density over the oceans. Zone of enhanced risk of the negative ionosphere storms in Antarctica is congruent with depressed Antarctic South Auroral Electrojet, SAE, index as compared with the North Auroral Electrojet, NAE, index under the storm conditions [29] indicating strong asymmetries between the two hemispheres. The regions of persistent perturbations of the ionosphere don't coincide with the regional anomalies in the ionosphere structure such as Weddell Sea and Yakutsk anomalies or regions of strong / weak coupling of TEC [30,31].
4. As distinct from geomagnetic activity depicting maximum at equinoxes, the pW^+ and pW^- do not depict equinoctial maximum but winter maximum of pW^+ and summer maximum of pW^- are obtained under Wp storm conditions decreasing from high latitudes to minimum at equator throughout all seasons in the both hemispheres.
5. While pW^+ and pW^- reach 20-25% under Wp storm conditions, the spatial occurrence of pW^+ and pW^- comprise 6% at Southern hemisphere high latitudes based on more than 130,000 W-index maps under non-storm conditions. This result indicates that persistent storm signatures are always present in the 'quiet' ionosphere of auroral region that implies a potential risk for the ionosphere weather.

ACKNOWLEDGEMENTS

The GIM-TEC maps are provided by Jet Propulsion Laboratory at ftp://cddis.gsfc.nasa.gov/pub/gps/products/ionex/ .The global W index maps are provided at http://www.izmiran.ru/services/iweather/ and http://www.ionolab.org/. Catalogue of Wp storms is provided at http://www.izmiran.ru/services/iweather/storm/.

COMPETING INTERESTS

Authors have declared that no competing interests exist.

REFERENCES

1. Manucci AJ, Wilson BD, Yuan DN, Ho CM, Lindqwister UJ, Runge TF. A global mapping technique for GPS-derived ionospheric total electron content measurements. Radio Sci. 1998;33:565-582.
2. Mannucci AJ, Tsurutani BT, Abdu MA, Gonzales WD, Komjathy A, Echer E, Ijima BA, Crowley G, Anderson D. Superposed epoch analysis of the dayside ionospheric response to four intense geomagnetic storms. J. Geophys. Res. 2008;113: A00A02.
   DOI:10.1029/2007JA012732.
3. Zhao B, Wan W, Liu L, Mao T. Morphology in the total electron content under geomagnetic disturbed conditions: Results from global ionosphere maps. Ann. Geophys. 2007;25:1555-1568.
   Available:www.ann-geophys.net/25/1555/2007/
4. Hernandez-Pajares M, Juan JM, Sanz J, Garcia-Rigo A, Feltens J, Komjathy A, Schaer SC, Krankowski A. The IGS VTEC maps: A reliable source of ionospheric information since 1998. J. Geodesy. 2009; 83:263-275.
5. Liu J, Zhao B, Liu L. Time delay and duration of the ionospheric total electron content responses to geomagnetic disturbances. Ann. Geophys. 2010;28: 795–805.
   Available:www.ann-geophys.net/28/795/2010/
6. Gulyaeva T, Veselovsky IS. Two-phase storm profile of global electron content in the ionosphere and plasmasphere of the

earth. J. Geophys. Res. Space Phys. 2012;117:A09325.
DOI:10.1029/2012JA018017.

7. Immel TJ, Manucci AJ. Ionospheric redistribution during geomagnetic storms. J. Geophys. Res., Space Phys. 2013;118: 7928-7939.
DOI:10.1002/2013JA018919.
8. Dmitriev AV, Huang CM, Brahmanandam PS, Chang LC, Chen KT, Tsai LC. Longitudinal variations of positive dayside ionospheric storms related to recurrent geomagnetic storms. J. Geophys. Res. Space Phys. 2013;118:6806–6822.
DOI:10.1002/jgra.50575.
9. Mukhtarov P, Andonov B, Pancheva D. Global empirical model of TEC response to geomagnetic activity. J. Geophys. Res. Space Phys. 2013;118:6666-6685.
DOI:10.1002/jgra.50576.
10. Jakowski N, Stankov SM, Schlueter S, Klaehn D. On developing a new ionospheric perturbation index for space weather operations. Adv Space Res. 2006; 38:2596-2600.
DOI:10.1016/j.asr.2005.07.043.
11. Gulyaeva TL, Arikan F, Hernandez-Pajares M, Stanislawska I. GIM-TEC adaptive ionospheric weather assessment and forecast system. J. Atmosph. Solar-Terr. Phys. 2013;102:329-340.
DOI:10.1016/j.jastp.2013.06.011.
12. Gulyaeva TL, Arikan F, Hernandez-Pajares M, Veselovsky IS. North-south components of the annual asymmetry in the ionosphere. Radio Sci. 2014;49:485-496.
DOI:10.1002/2014RS005401.
13. Gulyaeva TL, Stanislawska I. Derivation of a planetary ionospheric storm index. Ann. Geophys. 2008;26:2645-2648.
Available:www.ann-geophys.net/26/2645/2008/
14. Gulyaeva TL, Stanislawska I. Magnetosphere associated storms and autonomous storms in the ionosphere-plasmasphere environment. J. Atmos. Solar-Terr. Phys. 2010;72:90-96.
DOI:10.1016/j.jastp.2009.10.012.
15. Gulyaeva, TL, Arikan F, Stanislawska I. Inter-hemispheric imaging of the ionosphere with the upgraded IRI-Plas model during the space weather storms. Earth, Planets and Space. 2011;63:929-939.
DOI:10.5047/eps.2011.04.007.
16. Kouris SS, Fotiadis DN, Zolesi B. Specifications of the F region variations for quiet and disturbed conditions. Phys. Chem. Earth Part C. 1999;24:321-327.
17. Mendillo M. Storms in the ionosphere: patterns and processes for total electron content. Reviews of Geophys. 2006;47: RG2001.
DOI:10.1029/2005RG000193.
18. Vijaya LD, Balan N, Ram ST, Liu, JY. Statistics of geomagnetic storms and ionospheric storms at low and mid latitudes in two solar cycles. J. Geophys. Res. Space Phys. 2011;16:A11.
DOI:10.1029/2011JA017042.
19. Mikhailov AV, Depueva AH, Leschinskaya TYu. Morphology of quiet time F2-layer disturbances: High and lower latitudes. Int. J. Geomag. Aeronom. 2004;1–14:GI1006.
DOI:10.1029/2003GI000058
20. Deminov MG, Deminova GF, Zherebtsov GA, Polekh NM. Statistical properties of variability of the quiet ionosphere F2-layer maximum parameters over Irkutsk under low solar activity. Adv. Space Res. 2013;51:702-711.
DOI:10.1016/j.asr.2012.09.037.
21. Gulyaeva TL, Arikan F, Stanislawska I. Probability of occurrence of planetary ionosphere storms associated with the magnetosphere disturbance storm time events. Adv.Radio Sci. 2014;12:261-266.
DOI:10.5194/ars-12-261-2014.
Available:http://www.adv-radio-sci.net/12/261/2014/ars-12-261-2014.pdf
22. Mendillo M, Narvaez C. Ionospheric storms at geophysically-equivalent sites – Part 1: Storm-time patterns for sub-auroral ionospheres. Ann. Geophys. 2009;27: 1679–1694.
DOI: 10.5194/angeo-27-1679-2009.
23. Loewe CA, Prölss GW. Classification and mean behavior of magnetic storms. J. Geophys. Res. Space Phys. 1997;102:A7, 14209-14214.
DOI:10.1029/96JA04020.
24. Fotiadis DN, Kouris SS. A functional dependence of foF2 variability on latitude. Adv. Space Res. 2006;37:1023–1028.
25. Bencze P. Geographical distribution of long-term changes in the height of the maximum electron density of the F region: A nonmigrating-tide effect? J. Geophys. Res. Space Phys. 2009;114:A06304.
DOI:10.1029/2008JA013492.
26. Förster M, Cnossen I. Upper atmosphere differences between northern and southern

high latitudes: The role of magnetic field asymmetry. J. Geophys. Res. Space Physics. 2013;118:5951-5966. DOI:10.1002/jgra.50554.

27. Triskova L. The vernal-autumnal asymmetry in the seasonal variation of geomagnetic activity. J. Atmosph. Terr. Phys. 1989;51:111-118.
28. Mikhailov AV, Depuev VH, Depueva AH. Synhchronous *Nm*F2 and *Nm*E daytime variations as a key to the mechanism of quiet-time F2-layer disturbances. Ann. Geophys. 2007;25:483–493. Available:www.ann-geophys.net/25/483/2007/
29. Weygand JM, Zesta E, Troshichev O. Auroral electrojet indices in the Northern and Southern Hemispheres: A statistical comparison. J. Geophys. Res. Space Phys. 2014;119:4819–4840. DOI:10.1002/2013JA019377.
30. Klimenko MV, Klimenko VV, Karpachev AT, Ratovsky KG, Stepanov AE. Spatial features of Weddell Sea and Yakutsk Anomalies in foF2 diurnal variations during high solar activity periods: Interkosmos-19 satellite and ground-based ionosonde observations, IRI reproduction and GSM TIP model simulation. Adv. Space Res. 2015;55:2020–2032.
31. Yasukevich YuV, Zhivetiev IV. Using network technology for studying the ionosphere. A Review Solar-Terrestrial Physics. 2015;1:3 (in press).

Peer-review history:
The peer review history for this paper can be accessed here:
http://sciencedomain.org/review-history/11617